Monthly Notices
of the
ROYAL ASTRONOMICAL SOCIETY

MNRAS **451,** 739–750 (2015) doi:10.1093/mnras/stv895

MAGIC detection of short-term variability of the high-peaked BL Lac object 1ES 0806+524

J. Aleksić,[1] S. Ansoldi,[2] L. A. Antonelli,[3] P. Antoranz,[4] A. Babic,[5] P. Bangale,[6] J. A. Barrio,[7] J. Becerra González,[8⋆] W. Bednarek,[9] E. Bernardini,[10] B. Biasuzzi,[2] A. Biland,[11] O. Blanch,[1] S. Bonnefoy,[7] G. Bonnoli,[3] F. Borracci,[6] T. Bretz,[12†] E. Carmona,[13] A. Carosi,[3] P. Colin,[6] E. Colombo,[8] J. L. Contreras,[7] J. Cortina,[1] S. Covino,[3] P. Da Vela,[4] F. Dazzi,[6] A. De Angelis,[2] G. De Caneva,[10] B. De Lotto,[2] E. de Oña Wilhelmi,[14] C. Delgado Mendez,[13] F. Di Pierro,[3] D. Dominis Prester,[5] D. Dorner,[12] M. Doro,[15] S. Einecke,[16] D. Eisenacher,[12] D. Elsaesser,[12] A. Fernández-Barral,[1] D. Fidalgo,[7] M. V. Fonseca,[7] L. Font,[17] K. Frantzen,[16] C. Fruck,[6] D. Galindo,[18] R. J. García López,[8] M. Garczarczyk,[10] D. Garrido Terrats,[17] M. Gaug,[17] N. Godinović,[5] A. González Muñoz,[1] S. R. Gozzini,[10] D. Hadasch,[14‡] Y. Hanabata,[19] M. Hayashida,[19] J. Herrera,[8] J. Hose,[6] D. Hrupec,[5] W. Idec,[9] V. Kadenius,[20] H. Kellermann,[6] M. L. Knoetig,[11] K. Kodani,[19] Y. Konno,[19] J. Krause,[6] H. Kubo,[19] J. Kushida,[19] A. La Barbera,[3] D. Lelas,[5] N. Lewandowska,[12] E. Lindfors,[20§] S. Lombardi,[3] F. Longo,[2] M. López,[7] R. López-Coto,[1] A. López-Oramas,[1] E. Lorenz,[6] I. Lozano,[7] M. Makariev,[21] K. Mallot,[10] G. Maneva,[21] K. Mannheim,[12] L. Maraschi,[3] B. Marcote,[18] M. Mariotti,[15] M. Martínez,[1] D. Mazin,[6] U. Menzel,[6] J. M. Miranda,[4] R. Mirzoyan,[6] A. Moralejo,[1] P. Munar-Adrover,[18] D. Nakajima,[19] V. Neustroev,[20] A. Niedzwiecki,[9] M. Nievas Rosillo,[7] K. Nilsson,[20§] K. Nishijima,[19] K. Noda,[6] R. Orito,[19] A. Overkemping,[16] S. Paiano,[15] M. Palatiello,[2] D. Paneque,[6] R. Paoletti,[4] J. M. Paredes,[18] X. Paredes-Fortuny,[18] M. Persic,[2,22] J. Poutanen,[20] P. G. Prada Moroni,[23] E. Prandini,[11,24] I. Puljak,[5] R. Reinthal,[20¶] W. Rhode,[16] M. Ribó,[18] J. Rico,[1] J. Rodriguez Garcia,[6] T. Saito,[19] K. Saito,[19] K. Satalecka,[7] V. Scalzotto,[15] V. Scapin,[7] C. Schultz,[15¶] T. Schweizer,[6] S. N. Shore,[23] A. Sillanpää,[20] J. Sitarek,[1] I. Snidaric,[5] D. Sobczynska,[9] A. Stamerra,[3] T. Steinbring,[12] M. Strzys,[6] L. Takalo,[20] H. Takami,[19] F. Tavecchio,[3¶] P. Temnikov,[21] T. Terzić,[5] D. Tescaro,[8] M. Teshima,[6] J. Thaele,[16] D. F. Torres,[25] T. Toyama,[6] A. Treves,[26] P. Vogler,[11] M. Will,[8] R. Zanin,[18] K. Berger,[27] S. Buson,[15¶] F. D'Ammando,[28] D. Gasparrini,[29,30] T. Hovatta,[31,32] W. Max-Moerbeck,[33] A. Readhead[32] and J. Richards[34]

Affiliations are listed at the end of the paper

Accepted 2015 April 20. Received 2015 April 13; in original form 2014 November 12

⋆Present address: NASA Goddard Space Flight Center, Greenbelt, MD 20771, USA and Department of Physics and Department of Astronomy, University of Maryland, College Park, MD 20742, USA.
† Ecole polytechnique fédérale de Lausanne (EPFL), Lausanne, Switzerland.
‡ Institut für Astro- und Teilchenphysik, Leopold-Franzens-Universität Innsbruck, A-6020 Innsbruck, Austria.
§ Finnish Centre for Astronomy with ESO (FINCA), Turku, Finland.
¶ E-mail: rirein@utu.fi (RR); cornelia.schultz@pd.infn.it (CS); fabrizio.tavecchio@brera.inaf.it (FT); sara.buson@pd.infn.it (SB)

ABSTRACT

The high-frequency-peaked BL Lac (HBL) 1ES 0806+524 ($z = 0.138$) was discovered in very high energy (VHE) γ-rays in 2008. Until now, the broad-band spectrum of 1ES 0806+524 has been only poorly characterized, in particular at high energies. We analysed multiwavelength observations from γ-rays to radio performed from 2011 January to March, which were triggered by the high activity detected at optical frequencies. These observations constitute the most precise determination of the broad-band emission of 1ES 0806+524 to date. The stereoscopic Major Atmospheric Gamma-Ray Imaging Cherenkov (MAGIC) observations yielded a γ-ray signal above 250 GeV of (3.7 ± 0.7) per cent of the Crab Nebula flux with a statistical significance of 9.9σ. The multiwavelength observations showed significant variability in essentially all energy bands, including a VHE γ-ray flare that lasted less than one night, which provided unprecedented evidence for short-term variability in 1ES 0806+524. The spectrum of this flare is well described by a power law with a photon index of 2.97 ± 0.29 between $\sim$150 GeV and 1 TeV and an integral flux of (9.3 ± 1.9) per cent of the Crab nebula flux above 250 GeV. The spectrum during the non-flaring VHE activity is compatible with the only available VHE observation performed in 2008 with VERITAS when the source was in a low optical state. The broad-band spectral energy distribution can be described with a one-zone synchrotron self-Compton model with parameters typical for HBLs, indicating that 1ES 0806+524 is not substantially different from the HBLs previously detected.

Key words: radiation mechanisms: non-thermal – galaxies: active – BL Lacertae objects: individual: 1ES 0806+524 – galaxies: jets – gamma rays: galaxies.

1 INTRODUCTION

Active galactic nuclei (AGNs) are among the most variable objects in our Universe. Their broad-band energy spectrum spanning from radio to very high energy (VHE, $E > 100$ GeV) γ-rays can be characterized by two distinct peaks: one in the sub-mm to X-ray range, commonly interpreted as synchrotron radiation, and a second one in the γ-ray band that is hypothesized to originate from inverse Compton scattering of photons. The emission is assumed to originate from relativistic particle jets launched along the axis of the accretion disc of matter that surrounds a supermassive black hole (e.g. Blandford & Rees 1974). Numerous AGNs are known to be blazars, characterized by relativistic jets closely aligned to the line of sight of the observer. Based on their optical spectra, blazars are divided into two classes: flat spectrum radio quasars (FSRQs) that show broad emission lines, and BL Lacertae objects (BL Lacs) characterized by the weakness or even absence of such emission lines (Weymann et al. 1991; Stickel et al. 1991). Depending on the frequency of the low-energy peak of the spectral energy distribution (SED), the latter class is subdivided into high-frequency-peaking BL Lac object (HBL), intermediate- and low-frequency-peaking BL Lac objects (Padovani & Giommi 1995). The Tuorla Blazar Monitoring Program (Takalo et al. 2008) monitors a sample of objects in the optical band, triggering VHE observations by MAGIC telescopes during high optical states (Albert et al. 2006, 2007b, 2008a; Anderhub et al. 2009; Aleksić et al. 2012b,c). This allowed the discovery in VHE γ-rays of several blazars, especially HBLs and leads to the suggestion that in HBLs a high optical state is typically accompanied by a high state in VHE γ-rays. In some cases, studies of broad-band emission confirm a possible connection between the two wavebands (e.g. Aharonian et al. 2009; Aleksić et al. 2012d) whereas in other sources this seems to be only partially the case (e.g. Foschini et al. 2007, 2008).

1ES 0806+524 (RA 08:09:49.18673, Dec. 52:18:58.2507; J2000; Petrov & Taylor 2011) is classified as a BL Lac (Schachter et al. 1993) with a redshift of 0.138 (Bade et al. 1998). It was suggested as a VHE candidate (Costamante & Ghisellini 2002) with a predicted intrinsic flux of $F_{E>0.3\,\mathrm{TeV}} = 1.36 \times 10^{-11}\,\mathrm{cm}^{-2}\,\mathrm{s}^{-1}$. Several VHE observations have been carried out by the Whipple Collaboration and the HEGRA Collaboration yielding flux upper limits above 300 GeV (de la Calle Pérez et al. 2003; Horan et al. 2004) and 1.09 TeV (Aharonian et al. 2004), respectively.

In 2008, the Very Energetic Radiation Imaging Telescope Array System (VERITAS) Collaboration reported the first detection of 1ES 0806+524 in the VHE γ-ray band (Acciari et al. 2009). The collected data set spanned from 2006 November to 2008 April yielding a total of 245 excess events with a significance of 6.3σ. The integral flux above 300 GeV corresponded to 1.8 per cent of the Crab nebula flux, which is below earlier upper limits obtained by MAGIC-I observations in 2005 (5.6 per cent C.U.[1] above 230 GeV; Albert et al. 2008d; 7.2 per cent C.U. above 140 GeV; Aleksić et al. 2011). No significant variability on a monthly time-scale (the χ^2/d.o.f.[2] for a fit with a constant is 6.78/5; Acciari et al. 2009) could be established for this object. The spectrum was obtained only for a subset of data taken with four telescopes during winter 2007/2008. Accordingly, the spectral characteristics were poorly defined. Thus, the spectral index was measured to be $3.6 \pm 1.0_{\mathrm{stat}} \pm 0.3_{\mathrm{sys}}$ in a narrow range between 300 and 700 GeV. The time-independent version of the one-zone jet radiation transfer code of Böttcher & Chiang (2002), with parameters appropriate for a pure synchrotron self-Compton (SSC) model (Maraschi & Tavecchio 2003) was able to describe the data sufficiently well within the uncertainties.

In this paper, we report the highly significant detection of this source with the MAGIC stereoscopic system during a flaring state in 2011 February. We analyse in detail the variability and the spectral evolution of the source and present complementary data from

[1] The integrated flux level in Crab units (C.U.s) is obtained by normalizing the integrated flux measured above a certain threshold to the Crab nebula flux, which is considered to be stable, measured above the same threshold.
[2] d.o.f. = degrees of freedom.

observations in high-energy (HE, 30 MeV < E < 100 GeV) γ-rays carried out by the *Fermi* Large Area Telescope (LAT), in X-rays performed by the *Swift* satellite and in the optical R band by the Kungliga Vetenskapsakademien (KVA) telescope. Radio data coverage is provided by the Owens Valley Radio Observatory (OVRO) telescope at 15 GHz. Thanks to the good multiwavelength (MWL) coverage, we investigate the connection among these wavebands. Finally, we model the SED including all MWL data.

2 OBSERVATION AND DATA ANALYSIS

2.1 MAGIC observations and data analysis

Since 2009 MAGIC has operated as a stereoscopic system of two 17 m Imaging Atmospheric Cherenkov Telescopes located at the Roque de Los Muchachos, La Palma, Canary Islands (28.8 N, 17.9 W, 2225 m a.s.l.). Due to its low energy threshold (as low as 60 GeV in normal trigger mode) and high sensitivity,[3] it is a well-suited instrument for VHE γ-ray observations of blazars.

MAGIC observed 1ES 0806+524 between 2011 January and March on 13 nights for a total exposure of ∼24 h. The observations from February to March were triggered by a flux increase in the optical R band as part of a dedicated MAGIC Target of Opportunity (ToO) program to observe blazars showing high activity at other wavelengths. After applying quality selection cuts based on the event rate, ∼3.8 h of data were discarded. Additionally, corrections for the dead time of the readout system yielded an effective observation time of 16.1 h. Part of the observations were carried out under moderate moonlight conditions.

Observations were performed in the so-called *wobble* mode (Fomin et al. 1994) during which both telescopes alternated every 20 min between two sky positions with an offset of 0.4 from the source. The acquired data cover a zenith angle from 23° to 46°.

The data analysis was performed using the MAGIC standard tool 'MARS' (Moralejo et al. 2009) including adaptations to stereoscopic observations. Based on the timing information (Aliu et al. 2009), and absolute cleaning levels, the image cleaning was performed. The images were parametrized in each telescope individually according to the description of Hillas (Hillas 1985).

For the reconstruction of the shower arrival direction the random forest regression method (RF DISP method; Aleksić et al. 2010) with the implementation of stereoscopic parameters such as the impact distance of the shower on the ground and the height of the shower maximum was used (Lombardi et al. 2011).

To perform the gamma-hadron separation, the random forest method was applied (Albert et al. 2008b) using the image parameters of both telescopes and the shower impact point and height maximum. Energy lookup tables were used for the energy reconstruction. An angular resolution of ∼0.07 at 300 GeV and an energy resolution as good as 16 per cent in the medium energy range (few hundred GeV) are achieved (details on the stereo MAGIC analysis can be found in Aleksić et al. 2012a).

For sources with VHE γ-ray spectra similar to that of the Crab nebula, the sensitivity of the MAGIC stereo system is best above 250–300 GeV. For sources with spectral shapes softer than that of the Crab nebula, the best performance occurs at slightly lower energies. Consequently, we chose 250 GeV as the minimum energy to report signal significances and γ-ray fluxes in light curves, while for the spectral analysis, in order to use all the available information, we also considered energies well below 250 GeV, where the analysis of the MAGIC data can still be performed.

[3] Better than 0.8 per cent of the Crab nebula flux in 50 h of observing time above 290 GeV (Aleksić et al. 2012a).

2.2 *Fermi*-LAT data analysis

1ES 0806+524 has been observed by the pair conversion telescope *Fermi*-LAT optimized for energies from 20 MeV up to energies beyond 300 GeV (Atwood et al. 2009). In survey mode, the *Fermi*-LAT scans the entire sky every 3 h. The data sample, which consists of observations between 2010 November 22 and 2011 June 13, was analysed with the standard analysis tool *gtlike*, part of the *Fermi* Science Tools software package (version 09-27-01) available from the *Fermi* Science Support Center.[4]

We selected P7CLEAN events located in a circular region of interest (ROI) of 10° radius centred on the position of 1ES 0806+524. To reduce the contamination from the Earth-limb γ-rays produced by cosmic ray interactions with the upper atmosphere, data were restricted to a maximum zenith angle of 100°.

For the γ-ray signal extraction, the background model used included two components: Galactic diffuse and an isotropic diffuse emission, provided by the publicly available files gal_2yearp7v6_trim_v0.fits and iso_p7v6clean.txt.[5]

The model of the ROI also included sources from the second *Fermi*-LAT catalogue (2FGL; Nolan et al. 2012) that are located within 15° of 1ES 0806+524. These sources, as well as the source of interest, were modelled with a power-law spectral shape with the initial parameters set to their 2FGL values. In the 2FGL catalogue, 1ES 0806+524 is associated with the source 2FGL J0809.8+5218, which has been reported with a flux of $(2.2 \pm 0.3) \times 10^{-8}$ cm^{-2} s^{-1} and a photon index of (1.94 ± 0.06) in the 2FGL catalogue. When fitting, the spectral parameters of sources within 10° from our target were allowed to vary while those within 10°–15° were fixed to their initial values.

During the spectral fitting, the normalizations of the background models were allowed to vary freely. Spectral parameters were estimated from 300 MeV to 300 GeV using an unbinned maximum likelihood technique (Mattox et al. 1996) taking into account the post-launch instrument response functions (specifically P7CLEAN_V6; Ackermann et al. 2012).

During the MAGIC observing period, the source was not significantly detected on a daily basis. To ensure a good compromise between having a significant detection in most of the intervals and details on the temporal behaviour of the source, the light curve was produced with weekly binning. Flux upper limits at 95 per cent confidence level were calculated for each time bin where the test statistic (TS[6]) value for the source was below 9 (see Section 3.2).

The systematic uncertainty in the flux is dominated by the systematic uncertainty in the effective area, which is estimated to be 10 per cent at 100 MeV, decreasing to 5 per cent at 560 MeV, and increasing to 10 per cent at 10 GeV (Ackermann et al. 2012). The

[4] http://fermi.gsfc.nasa.gov/ssc/

[5] http://fermi.gsfc.nasa.gov/ssc/data/access/lat/BackgroundModels.html

[6] The test statistic value quantifies the probability of having a pointlike γ-ray source at the location specified. It corresponds roughly to the standard deviation squared assuming one degree of freedom (Mattox et al. 1996). The TS is defined as $-2\log(L_0/L)$, where L_0 is the maximum likelihood value for a model without an additional source (i.e. the 'null hypothesis') and L is the maximum likelihood value for a model with the additional source at the specified location.

systematic uncertainties are smaller than the statistical uncertainties of the data points in the light curve and spectra.

2.3 *Swift* observations and analysis

Beside its prime objective of detecting and following up γ-ray bursts, since its launch in 2004 November the *Swift* Gamma-Ray Burst observatory has become an instrument suitable for various purposes due to its fast response and its MWL abilities (Gehrels et al. 2004). *Swift* hosts three telescopes optimized for different energy ranges: the Burst Alert Telescope (Barthelmy et al. 2005) suited for observations between 15 and 150 keV, the X-ray telescope (XRT; Burrows et al. 2005) with a 0.3–10 keV coverage and the UV/Optical Telescope (UVOT; Roming et al. 2005) optimal for observations within the 1800–6000 Å wavelength range.

Following the VHE γ-ray flare detection of 1ES 0806+524 by MAGIC (Mariotti 2011), *Swift* ToO observations were requested and performed from 2011 February 26 to March 2; five observations together with MAGIC. A high-activity state of the source was confirmed reporting clear variability in X-rays (Stamerra et al. 2011). The source was monitored with the *Swift*/XRT in photon counting (PC) mode with ∼2 ks snapshots each night for a total exposure time of 10 ks.

The data processing was performed with the XRTPIPELINE v0.12.6 distributed by HEASARC as part of the HEASOFT package. Events with grades 0–12 (according to the *Swift* nomenclature; Burrows et al. 2005) were selected for the PC data and the response matrices included in the *Swift* CALDB[7] were applied. All observations showed a source count rate >0.5 counts s^{-1}, thus pile-up correction was required. We extracted the source events from an annular region with an inner radius of 3 pixels (estimated by means of the point spread function (PSF) fitting technique; see Moretti et al. 2005) and an outer radius of 30 pixels, while background events were extracted from an annular region centred on the source with radii of 70 and 120 pixels. Ancillary response files were generated with XRTMKARF, and account for different extraction regions, vignetting and PSF corrections.

We fit the spectra in the 0.3–10 keV energy range. The spectra were rebinned with a minimum of 20 counts per energy bin so that the χ^2 minimization fitting technique could be used. The spectral analysis was performed with XSPEC (Arnaud 1996) adopting a simple power-law model that includes a hydrogen-equivalent column density fixed to the Galactic value $n\mathrm{H} = 4.1 \times 10^{20}\,\mathrm{cm}^{-2}$ (Kalberla et al. 2005).

Swift/UVOT data were taken with the 'filter of the day' (either *U*, *UVW*1, *UVM*2 or *UVW*2 filter; Poole et al. 2008) chosen day by day by the *Swift* science planners. We analysed the data using the `uvotsource` task included in the HEASOFT package. Source counts were extracted from a circular region of 5 arcsec radius centred on the source, while background counts were derived from a circular region of 10 arcsec radius in the source neighbourhood. Conversion of magnitudes into dereddened flux densities was obtained by adopting the extinction value $E(B-V) = 0.039$ from Schlegel, Finkbeiner & Davis (1998), the mean Galactic extinction curve in Fitzpatrick (1999) and the magnitude-flux calibrations by Bessell, Castelli & Plez (1998).

[7] http://heasarc.gsfc.nasa.gov/docs/heasarc/caldb/swift/

2.4 Optical observations and data analysis

The optical data used in this study were obtained with the KVA[8] located at the Roque de los Muchachos observatory on La Palma, and consisting of two telescopes mounted on the same fork. The smaller, a 35 cm Celestron, is used for photometric measurements, while the larger, a 60 cm one, is used for polarimetric observations. They are operated remotely from Finland. The photometric measurements are performed in the optical *R* band using differential photometry, by having the target and the calibrated comparison stars in the same CCD images (Fiorucci, Tosti & Rizzi 1998). The magnitudes of the source and comparison stars are measured using aperture photometry and converted to linear flux densities according to the formula $F(\mathrm{Jy}) = F_0 \times 10^{\mathrm{magR}/\,-\,2.5}$, where F_0 is a filter-dependent zero-point ($F_0 = 3080$ Jy in the *R* band; from Bessell 1979). To obtain the AGN core emission, contributions from the host galaxy and possible nearby stars that add to the overall flux have to be subtracted from the obtained value. These values were determined by Nilsson et al. (2007) and in the case of 1ES 0806+524 the host galaxy contribution of (0.69 ± 0.04) mJy was subtracted from the overall flux.

The KVA telescope is operated under the Tuorla Blazar Monitoring Program,[9] which has been running as a support program to the MAGIC observations since the end of 2002. The project uses the Tuorla 1 m (located in Finland) and the KVA telescopes to monitor candidates (from Costamante & Ghisellini 2002) and known TeV blazars in the optical waveband and to provide alerts to MAGIC on high states of these objects in order to trigger follow-up VHE observations. 1ES 0806+524 was one of the objects on the original target list and has therefore been monitored regularly since the beginning of the program. The object had been relatively dormant over the last years, showing some variability but no particular flaring activity. The large flare occurring at the end of 2010 (see Section 3.2) is by far the largest optical activity recorded from this source during the last 10 yr, although this kind of flaring activity is not uncommon in the optical light curves of other blazars observed within the Tuorla monitoring program.

2.5 OVRO data analysis

Observations at 15 GHz were carried out with the 40 m OVRO radio telescope, located in California. The observations of 1ES 0806+524 were carried out in the framework of a blazar monitoring program (Richards et al. 2011) measuring the source flux density twice a week. Occasional gaps in the data sample are due to poor weather conditions or maintenance. Observations were performed using a Dicke-switched dual-beam system, with a second level of switching in azimuth to alternate between source and sky in each of the two horns, which removes much of the atmospheric and ground interference (Readhead et al. 1989). The data were calibrated against 3C 286 with an assumed flux density of 3.44 Jy at 15 GHz (Baars et al. 1977). The data were analysed using the pipeline described in Richards et al. (2011).

[8] http://www.astro.utu.fi/telescopes/60lapalma.htm
[9] Project web page: http://users.utu.fi/kani/1m/

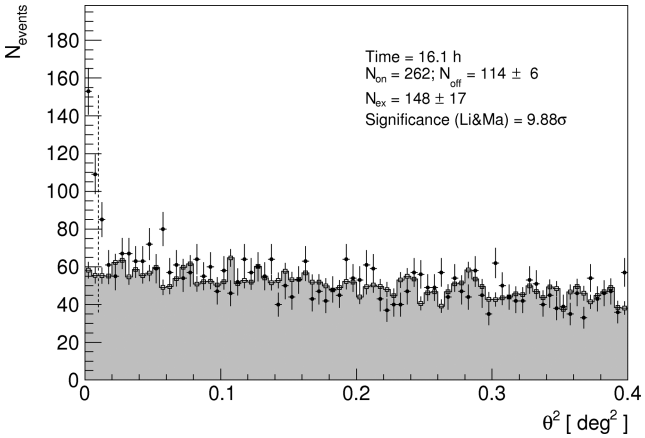

Figure 1. Distribution of the squared angular distance (θ^2) for the on-source counts in the direction of 1ES 0806+524 (black points with error bars) and the normalized off-source events (grey histogram and open black squares) extracted from three background regions which are located at 90°, 180° and 270° with respect to the reconstructed source position in the camera. The signal is extracted in the θ^2-region indicated by the vertical dashed line.

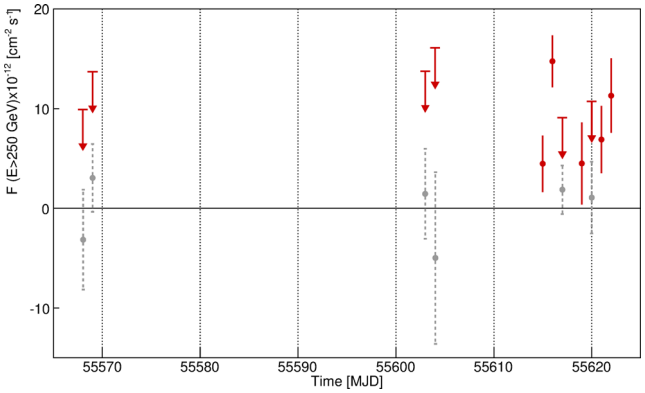

Figure 2. VHE γ-ray flux ($E > 250$ GeV) of 1ES 0806+524 for the single MAGIC observations performed in 2011. The red arrows correspond to 95 per cent confidence upper limits, which were computed for the observations where the interval flux ± error contains zero. The measured fluxes for these intervals are also shown (grey circles).

3 RESULTS

3.1 MAGIC results

Above an energy threshold of 250 GeV the MAGIC data yield (after event selection cuts) an excess of 148 ± 17 events in the distribution of the squared angular distance θ^2 between the reconstructed event direction and the catalogue position of 1ES 0806+524, i.e. in the so-called On region. The background level of 114 ± 6 events was calculated from three equivalent 'Off' regions, located at 90°, 180° and 270° with respect to the reconstructed source position in the camera, applying the same event selection cuts (Fig. 1).

The significance of the event excess corresponds to 9.9σ calculated with formula (17) of Li & Ma (1983). During the MAGIC observations, the source underwent a flaring event on February 24 (Mariotti 2011). Within 3.0 h of observation an excess of 50 ± 8 events (15 ± 2 background events) above 250 GeV was measured corresponding to a confidence level of 7.6σ. After excluding the flare of February 24 from the data set, the remaining MAGIC observations (13.1 h) still show a significant detection of 96 ± 15 excess events (99 ± 6 background events) above 250 GeV corresponding to 7.3σ. In the following, we will refer to the VHE γ-ray flare as the high state. The low state refers to a low activity in VHE γ-rays including the remaining MAGIC observations.

The integral flux above 250 GeV was (5.9 ± 1.1) × 10^{-12} cm^{-2} s^{-1} corresponding to (3.7 ± 0.7) per cent C.U. Excluding the flare, the integral flux was measured to be (3.1 ± 1.0) × 10^{-12} cm^{-2} s^{-1} corresponding to (1.9 ± 0.7) per cent C.U. (2.1 ± 0.7 per cent C.U. above 300 GeV). This result is in good agreement with the flux level above 300 GeV reported by VERITAS in 2009 (1.8 per cent C.U.; Acciari et al. 2009). During the night when the source was flaring the integral flux was (1.5 ± 0.3) × 10^{-11} cm^{-2} s^{-1} equal to (9.3 ± 1.9) per cent C.U. The flare showed a flux of ∼3σ above the mean flux level[10] which corresponded to a flux increase of about a factor of 3 (Fig. 2). No intra-night variability was found during the VHE γ-ray flare within the statistical and systematic uncertainties. Besides the first flare observed by MAGIC on 2011 February 24 (MJD = 55616), the VHE data showed a hint of increasing flux towards March 2 (MJD = 55622), when the source was detected at ∼5 σ with a flux of (7.0 ± 2.3) per cent C.U. above 250 GeV. Fitting the overall light curve with a constant function yields a probability of 0.5 per cent (χ^2/d.o.f. = 24.92/10) for a non-variable source. Since the nights before and after the flaring event of February 24 showed a significantly lower flux, we assume short-term variability of the time-scale of 1 d as an upper limit.

The differential energy spectra of the high and low states are shown in Figs 3 and 4, respectively. Both spectra can be described

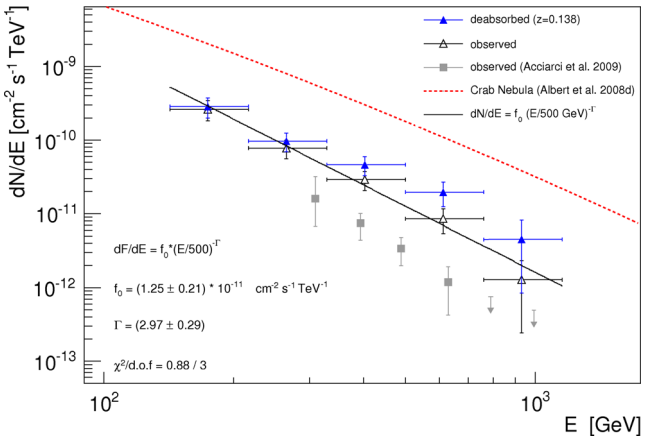

Figure 3. Unfolded high-state differential energy spectrum of 1ES 0806+524 measured by MAGIC on 2011 February 24. The open black triangles correspond to the measured spectrum to which a simple power law (filled black line) is fitted; the filled blue triangles depict the measured spectrum after correction for the EBL attenuation using the model by Domínguez et al. (2011). For comparison, the observed spectrum and derived upper limits (grey squares and arrows, respectively) published by VERITAS (Acciari et al. 2009) and the Crab nebula spectrum (red dashed line) published by MAGIC (Albert et al. 2008c) are shown. See text for further details.

[10] The deviation from the constant flux level was computed by dividing the difference of the flux measured during the VHE γ-ray flare and the mean flux level by the sum in quadrature of the statistical errors on the flux in the high and mean flux levels.

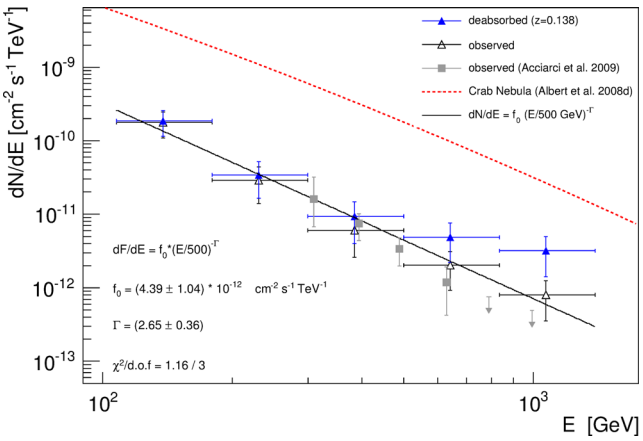

Figure 4. Unfolded low-state differential energy spectrum of 1ES 0806+524 measured by MAGIC in 2011. The open black triangles correspond to the measured spectrum to which a simple power law (filled black line) is fitted; the filled blue triangles depict the measured spectrum after correction for the EBL attenuation using the model by Domínguez et al. (2011). For comparison, the observed spectrum and derived upper limits (grey squares and arrows, respectively) published by VERITAS (Acciari et al. 2009) and the Crab nebula spectrum (red dashed line) published by MAGIC (Albert et al. 2008c) are shown.

with a simple power law[11] of the form $\mathrm{d}N/\mathrm{d}E = f_0(E/500\,\mathrm{GeV})^{-\Gamma}$ with a flux normalization f_0 at 500 GeV of $(1.25 \pm 0.21) \times 10^{-11}$ for the high and $(4.39 \pm 1.04) \times 10^{-12}$ cm^{-2} s^{-1} TeV^{-1} for the low state. The photon index Γ was found to be 2.97 ± 0.29 for the high and 2.65 ± 0.36 for the low state. The spectra have been unfolded using the Tikhonov algorithm to correct for the finite energy resolution of MAGIC. Different unfolding algorithms as described in Albert et al. (2007a) were compared and found to agree within errors.

To account for extragalactic background light (EBL) attenuation, a correction by means of the EBL model of Domínguez et al. (2011)[12] was applied. The corrected spectral flux of the two different source states follows a power law parametrized by a photon index $\Gamma = 2.30 \pm 0.52$ and 2.15 ± 0.59 as well as a flux normalization f_0 at 500 GeV $(2.57 \pm 0.81) \times 10^{-11}$ and $(9.10 \pm 4.03) \times 10^{-12}$ cm^{-2} s^{-1} TeV^{-1}, for the high (Fig. 3) and low states (Fig. 4), respectively. The low state spectrum observed by MAGIC shows a good agreement within errors with the observed spectral points published by VERITAS. A comparison of the differential energy spectra describing the different source states indicates an increase in flux but no significant hardening of the spectrum.

3.2 Multiwavelength results

Fig. 5 shows the long-term MWL light curves in VHE γ-rays (MAGIC), HE γ-rays (*Fermi*-LAT), X-rays (*Swift*), in the *R* band (KVA, Tuorla) and radio regime (OVRO telescope).

The *Fermi*-LAT light curve was produced fixing the power-law index of the source of interest to the value derived from the spectral analysis of the data set from 2010 November 22 to 2011 June 13, i.e. 1.88 ± 0.17.

[11] The fits of the high and low state spectra with a power law have a χ^2/d.o.f. of 0.88/3 (83 per cent) and 1.16/3 (76 per cent), respectively.

[12] This model is among the most recent ones (e.g. Franceschini, Rodighiero & Vaccari 2008; Finke, Razzaque &Dermer 2010; Gilmore et al. 2012) and agrees within the uncertainties with other models.

Possible variations in the source emission in HE γ-rays have been tested following the same likelihood method described in the 2FGL (Nolan et al. 2012). The method, applied to the data from 2010 November to 2011 June, indicates that the source is variable ($\mathrm{TS_{var}} = 52$ for 29 d.o.f.). When applied only to data taken during the MAGIC observation period (MJD = 55603 to MJD = 55622) the probability for constant emission increases to 23 per cent ($\mathrm{TS_{var}}$/d.o.f. = 10.5/8). Considering the entire data sample, i.e. from 2010 November 22 to 2011 June 13, the average flux level corresponds to $(2.10 \pm 0.14) \times 10^{-8}$ cm^{-2} s^{-1} ($E > 300$ MeV).

A smooth flux increase from the beginning of 2011 March until 2011 mid-April reaching a maximum of $(5.2 \pm 1.3) \times 10^{-8}$ cm^{-2} s^{-1} was observed with a delay compared to the other wavelengths. Given the long integration time of 7 d, no clear conclusion regarding simultaneous source variability with respect to that observed in VHE γ-rays can be drawn within the time interval of the flare. In particular, during the night of the VHE γ-ray flare the source was only marginally detected (TS = 4) in the *Fermi*-LAT energy band.

In order to provide simultaneous coverage in this energy band, we computed the 95 per cent confidence level upper limit between 300 MeV and 300 GeV for February 24 corresponding to 7.2×10^{-11} erg cm^{-2} s^{-1} at a centre energy of 580 MeV.

The X-ray spectra derived with the individual *Swift*/XRT observations are reported in Table 1. The time-averaged X-ray flux in the band 2–10 keV is $(5.1 \pm 0.2) \times 10^{-12}$ erg cm^{-2} s^{-1}, with a flux increase by about a factor of 6 when comparing the lowest flux (occurring on February 1) with the highest flux (occurring on March 2). A fit with a constant function yields χ^2/d.o.f. = 150/5, showing a clear X-ray variability and confirming the high-activity state of the source during the MAGIC observations performed at the end of February and beginning of March.

Swift/UVOT observations were carried out with different filters in the ultraviolet bands. The brightness of (14.4 ± 0.03) mag measured on March 2 in the *UVW2* and *UVM2* bands is almost unchanged with respect to February 1 where a brightness of (14.5 ± 0.03) mag was measured. However, 1ES 0806+524 appears about 1 mag brighter compared to the UV flux observed in 2008 March. During the observations, the UV band photometry is compatible with a constant flux within the errors.

In the *R* band, the core flux showed a large increase over the long-term base level starting from 2010 November (Fig. 6). In the subsequent months, the flux density continued to increase until reaching a maximum of (4.75 ± 0.09) mJy (host galaxy subtracted) in the night of 2011 February 24 during the outburst in VHE γ-rays; this was almost three times higher than the quiescent state of 1.72 mJy (Reinthal et al. 2012). Later, the flux level steadily decreased.

The long-term radio light curve is consistent with constant emission (probability of $\sim 6.2 \times 10^{-5}$; χ^2/d.o.f. = 61.25/25) with an average flux level of (0.136 ± 0.01) Jy. Considering only data taken during MAGIC observations (MJD = 55603 to MJD = 55622), the hypothesis of a non-variable emission at a mean flux level of 0.13 Jy has a probability of 75 per cent. Compared to 2010 November observations, the radio data show a marginal flux increase from 2011 mid-January to May, exceeding the mean flux level of the overall observation period.

3.3 Variability study across wavebands

To study the connection between variability patterns in individual wavebands, MWL data gathered during the MAGIC observations

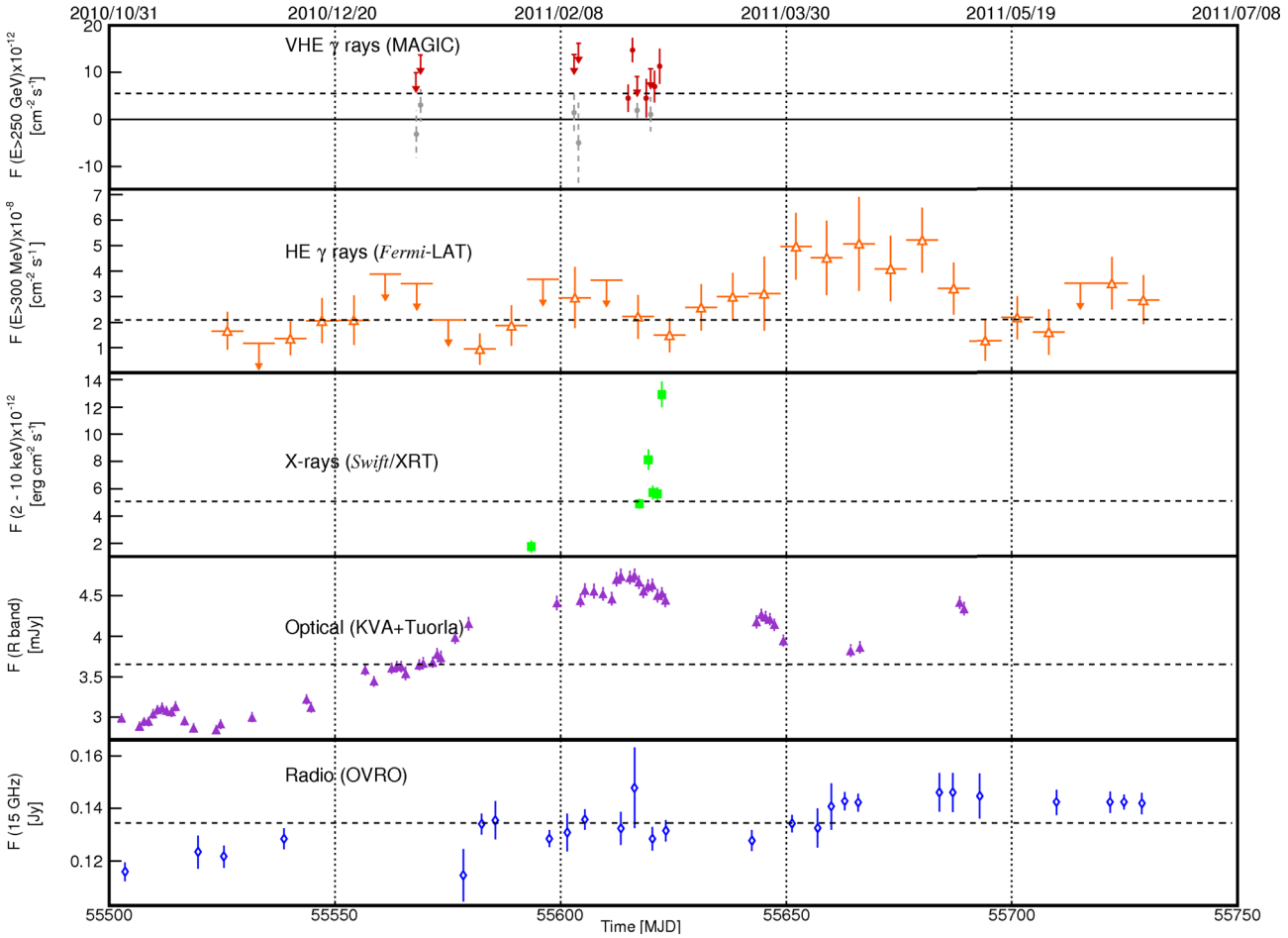

Figure 5. MWL light curves of 1ES 0806+524 from 2010 December to 2011 June. From top to bottom: VHE γ-rays (red circles) by MAGIC, HE γ-rays (orange triangles) by *Fermi*-LAT, X-rays (green squares) by *Swift*/XRT, *R* band (purple triangles) by KVA, and radio (blue diamonds) by OVRO. The optical data are corrected for the host galaxy contribution according to Nilsson et al. (2007). Upper limits at 95 per cent confidence level are indicated by downward arrows. In the VHE light curve, upper limits (red arrows) are computed for the observations where the interval flux ± error contains zero. The measured fluxes for these intervals are also shown (grey circles). The individual light curves are daily binned except for the light curve in the HE band from *Fermi*, where a binning of 1 d has been used. The horizontal dashed lines report the mean flux in each light curve.

Table 1. Log and fitting results of *Swift*/XRT observations of 1ES 0806+524 using a power-law model with $N_{\rm H}$ fixed to Galactic absorption in the range from 0.3 to 10 keV.

Observation Date [MJD]	Photon index Γ	Flux 2–10 keV $\times 10^{-12}$ erg cm^{-2} s^{-1}	χ^2/d.o.f.
55593	2.75 ± 0.30	1.76 ± 0.43	Cash[a]
55617	2.36 ± 0.09	4.91 ± 0.36	36.84/34
55619	2.44 ± 0.10	8.13 ± 0.73	27.73/27
55620	2.38 ± 0.09	5.73 ± 0.51	46.39/37
55621	2.40 ± 0.11	5.63 ± 0.49	33.67/27
55622	2.29 ± 0.08	12.92 ± 0.94	38.58/40

Note. [a]The Cash statistic (Humphrey, Liu & Buote 2009) was used to fit the spectrum.

(from MJD 55568 to MJD 55622) were studied. Due to the sparse overlap of simultaneous multifrequency data and the limited duration of the MWL observations, detailed methods such as, e.g. calculating cross-correlation functions of simultaneous data sets were not applicable. We therefore settled for a simple linear 2D-regression analysis where we plotted the simultaneous data points from one waveband as a function of flux in the comparison waveband.

MWL data from five different wavebands (radio, optical, X-rays, HE γ-rays and VHE γ-rays) were available for comparison. The HE γ-ray band was excluded due to the inability to detect 1ES 0806+524 with *Fermi*-LAT on day time-scales, as it was done in the other wavebands. The data in the optical, X-rays and VHE γ-rays were fairly simultaneous being on average less than 2 h and individually no more than 3.25 h apart, while they all had an offset of roughly 12 h with respect to the radio observations. In the case of two radio measurements (MJD = 55616.4 and MJD = 55620.4) there were two observations in other wavebands, performed with a gap of ∼12 h before and after the corresponding radio observation. In those cases, we calculated the estimated flux level of the comparison waveband at the time of the radio measurement assuming linear behaviour of the flux between the two points. This led to the exclusion of radio to X-ray and radio to VHE data sets from the study due to a low number of concurrent data points. In total, we have four waveband pairs for the study: radio versus optical, optical versus X-rays, optical versus VHE γ-rays and X-rays versus VHE γ-rays.

We settled on a 16 h window as a trade-off between strict simultaneity and feasible daily overlap for selecting the MWL correlation points. In practice, this only affected the comparison of radio to other

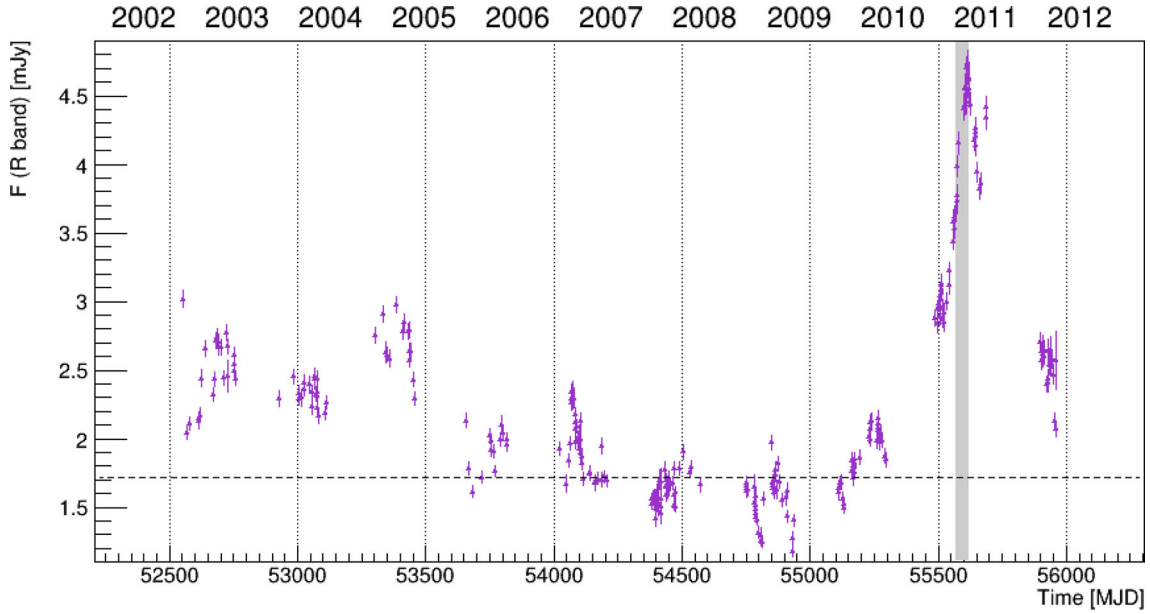

Figure 6. Host-galaxy-corrected (Nilsson et al. 2007) long-term light curve of 1ES 0806+524 of the optical *R* band observed by the KVA telescope. The grey shaded area marks the period of the MAGIC observations in 2011. The quiescent state (Reinthal et al. 2012) is indicated as a dashed line.

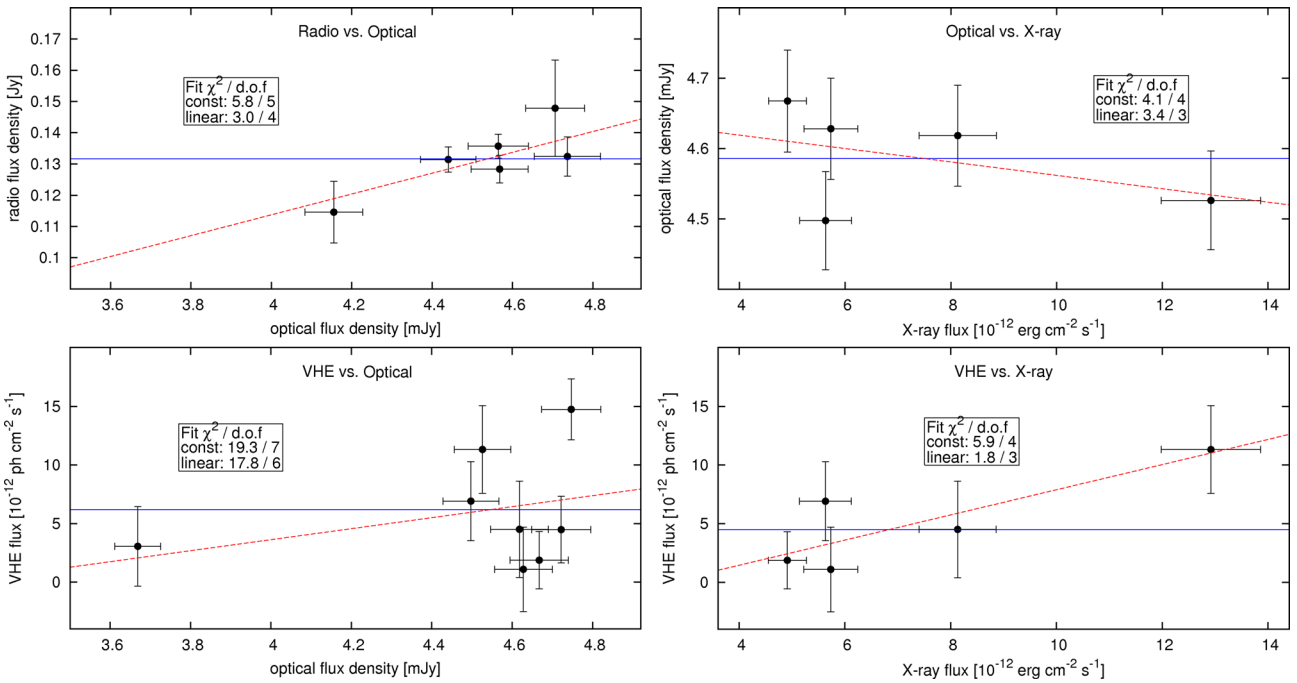

Figure 7. One-to-one connection plots derived for the MWL correlation studies carried out between VHE γ-rays, X-rays as well as the optical and radio bands. The data are marked in black (filled circles), while the constant and the linear fits are represented by blue filled and red dashed lines, respectively.

wavebands as all the rest of them had fairly simultaneous pointings. Nevertheless, the number of available points was quite low ranging from three to eight with radio to X-rays and radio to VHE having the lowest number of concurrent points. The result of this correlation study is shown in Fig 7.

In order to determine whether there is a correlation between activities in different wavebands, we compared the probability of a linear fit to the data to that of a constant fit (Table 2).

We find that the linear fits are not significantly better than the constant fits. The case with the largest difference occurs for the

Table 2. Results of the linear regression analysis.

	Optical to radio	Optical to X-ray	Optical to VHE	X-ray to VHE
χ^2/d.o.f (const. fit)	5.8/5	4.1/4	19.3/7	5.9/4
χ^2/d.o.f (lin. fit)	3.0/4	3.4/3	17.8/6	1.8/3
Fit likelihood (const. fit)	0.33	0.39	0.0073	0.21
Fit likelihood (lin. fit)	0.56	0.34	0.0068	0.62

X-ray to VHE flux, where a likelihood ratio test shows that the constant fit has a tail probability (computed using the Wilks theorem) of 0.04.

It is worth noting that, while the VHE observations were triggered by the optical high state, there seems to be no one-to-one correlation between the fluxes in the two wavebands in the short term. Focusing on observations right before and after the flare, optical observations indicate a rather constant flux while the measurements performed in VHE γ-rays lead to the derivation of a short-term variability on a daily time-scale. This suggests that the variability time-scales are very different in these two bands and for future studies a longer time span should be used.

4 SPECTRAL ENERGY DISTRIBUTION AND INTERPRETATION

The SED of the source describing the high and low source state during the MAGIC observations, together with contemporaneous data from *Fermi*, *Swift*, the KVA and OVRO telescopes are presented in Fig. 8. EBL corrections have been applied to the VHE γ-ray data using the model by Domínguez et al. (2011). *Swift*/UVOT data and optical data in the *R* band provided by the KVA telescope have been corrected for Galactic extinction and the host galaxy contribution, respectively, according to Fitzpatrick (1999) and Nilsson et al. (2007). Simultaneous and quasi-simultaneous data have been combined accordingly to the high and low state in VHE γ-rays. In general, quasi-simultaneous data have to be considered when studying the broad-band variability of blazars because strictly simultaneous observations are not always available. In this particular study, by quasi-simultaneous observations we mean the usage of *Swift* (X-ray and UV) data from 1 d after the VHE flare detected by MAGIC.

Unfortunately, the high state data do not include a simultaneous HE γ-ray detection, as *Fermi* did not significantly detect 1ES 0806+524 during the flares in VHE γ-rays and X-rays. In order to provide simultaneous coverage in this energy band, the 95 per cent confidence level upper limit (300 MeV to 300 GeV) for 2011 February 24 was included in the SED modelling (due to the poor statistics only one upper limit for the whole energy band has been calculated). In addition, an averaged SED from eight months of observations taken from 2010 November to 2011 June has been derived and is shown for comparison. Consequently, the latter data are not included in the modelling of the high state SED. For the low state of 1ES 0806+524, an averaged *Fermi* spectrum was produced considering data collected during the period from 2011 January to March 2 and excluding the night of the VHE γ-ray flare (February 24) from the data sample.

With respect to the *Swift* data, the high state comprises observations carried out on February 25 since it is the closest X-ray spectrum to the VHE flare detected by MAGIC on February 24, whereas the low state encompasses observations performed on February 1. Because of the high variability in the X-ray and VHE bands (especially during the flaring state), the lack of simultaneity between these two energy bands places uncertainty in the interpretation of the broad-band SEDs within the one-zone SSC model. Thus, we estimate the X-ray spectrum for February 24 by scaling the spectrum from February 25 (Fig. 5) with a factor of 3.3, which is derived from the linear fit to the X-ray-to-TeV flux (Fig. 7). Since we were not able to reproduce both the optical and VHE γ-ray SED points from previous MWL observations (Acciari et al. 2009), they are not shown.

The MAGIC observations show a clear flux variability of about a factor of 3 in VHE γ-rays when comparing the high and low states (see Figs 3 and 4). The *Fermi*-LAT light curve study indicated variability for the time period considered in this work (MJD = 55603 to MJD = 55622).

The *Swift*/XRT spectrum from February 25 is marginally harder than that from February 1, and the X-ray flux above 2 keV from February 25 is about three times higher than that from February 1 (Table 1). The ratio between the assumed X-ray spectrum for February 24 (high state) and the flux of February 1 (low state) is about nine.

The flux in the *R* band started to increase well before the flaring activity in the VHE regime and in X-rays (see Fig. 5). It reached a maximum level at an almost constant flux with only marginal variations towards the end of February when the VHE γ-ray flare

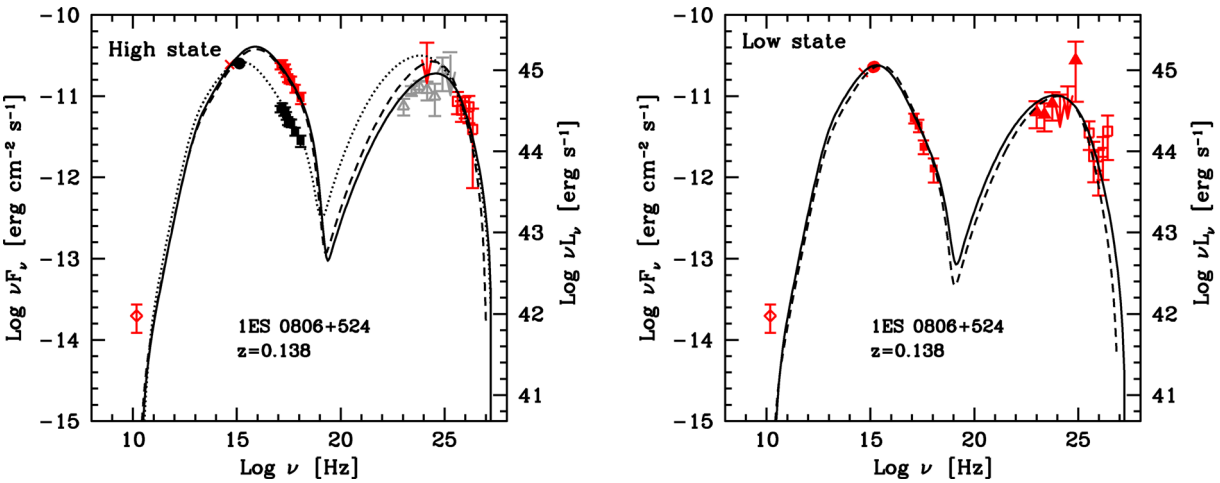

Figure 8. SED of the high (left) and low (right) states of 1ES 0806+524 obtained during the MAGIC observations. The red (black) markers depict the simultaneous (quasi-simultaneous from February 25) MWL data. The MAGIC VHE γ-ray data are shown with open squares, *Fermi*-LAT HE γ-ray data with triangles and arrows for the upper limits, *Swift*-XRT data with filled squares, *Swift*-UVOT data with filled circles, KVA data with crosses and OVRO data with open diamonds. The filled (dotted) black curve depicts the one-zone SSC model matching the simultaneous (quasi-simultaneous) data assuming a high Doppler factor. We also show the modelling (dashed line) of the simultaneous data assuming a lower Doppler factor. For comparison purposes, the left-hand panel shows also the *Fermi*-LAT HE γ-ray spectrum from 2010 November to 2011 June (grey open triangles and grey arrows). See text for further details.

Table 3. Input model parameters for the high and low state SEDs shown in Fig. 8. We report the minimum $\gamma_{\rm min}$, break $\gamma_{\rm b}$ and maximum Lorentz factor $\gamma_{\rm max}$ and the low- and high-energy slope of the electron energy distribution, the magnetic field intensity, the electron density, the radius of the emitting region and its Doppler factor. We also report the derived power carried by electrons, magnetic field and protons (assuming one cold proton per emitting relativistic electron and the frequencies of the synchrotron and inverse Compton peak). (I): high state with quasi-simultaneous X-ray data; (IIa/b): high state with assumed simultaneous X-ray data modelled with a high/low Doppler factor; (IIIa/b): low state modelled with a high/low Doppler factor.

$\gamma_{\rm min}$ [10^3]	$\gamma_{\rm b}$ [10^4]	$\gamma_{\rm max}$ [10^5]	n_1	n_2	B (G)	K [10^3 cm^{-3}]	R [10^{16} cm]	δ	$P_{\rm e}$ [10^{43} erg s^{-1}]	P_B [10^{43} erg s^{-1}]	$P_{\rm p}$ [10^{43} erg s^{-1}]	$\nu_{\rm sync}$ (Hz)	$\nu_{\rm IC}$ (Hz)	
1	1.65	7	2	3.85	0.05	19.0	1.12	30	79.9	0.1	28.9	$10^{15.26}$	$10^{23.84}$	(I)
1	3.2	7	2	3.85	0.06	3.0	1.70	30	34.3	0.35	11	$10^{15.97}$	$10^{24.61}$	(IIa)
1	3.6	7	2	3.85	0.10	2.6	3.00	15	24.0	0.76	7.3	$10^{15.90}$	$10^{24.48}$	(IIb)
1	2.1	7	2	4.15	0.05	4.0	1.70	30	43.0	0.2	14.3	$10^{15.33}$	$10^{23.87}$	(IIIa)
1	2.8	6	2	4.30	0.10	1.8	3.20	15	18.6	0.9	5.8	$10^{15.56}$	$10^{24.09}$	(IIIb)

occurred. Therefore, no clear variation between the high and low state SEDs is seen. While the inverse Compton peak indicates flux variability between both activity states, the synchrotron component shows only minor variation. Unfortunately, the weak detection in the HE γ-ray band limits the determination of the inverse Compton peak.

A one-zone SSC model is applied to reproduce the SEDs of both source states (for a detailed description of the model see Maraschi & Tavecchio 2003), where a spherical emission region of radius R is assumed, filled with a tangled magnetic field of intensity B. A population of relativistic electrons is approximated by a smoothed broken power law that is parametrized by the minimum $\gamma_{\rm min}$, break $\gamma_{\rm b}$ and maximum Lorentz factor $\gamma_{\rm max}$, as well as by the slopes n_1 and n_2 before and after the break, respectively. Relativistic effects are taken into account by the Doppler factor δ. The emission is self-absorbed at radio frequencies. This implies that the jet decelerates from the source region to the outer regions where the bulk of the radio emission originates. Therefore, radio data are not included in the SED modelling.

It is well known (Tavecchio, Maraschi & Ghisellini 1998) that the one-zone SSC model is constrained once the basic SED parameters and the variability time-scale $t_{\rm var}$ – related to the source radius – are known. In the case studied here only an upper limit on the variability time-scale is derived, $t_{\rm var} \lesssim 1$ d. This time-scale is much larger than the variability time-scale that has been measured during some flaring episodes in BL Lac objects, especially in the TeV band, for which sub-hour variability has been observed (Gaidos et al. 1996; Albert et al. 2007c; Aharonian et al. 2007). This uncertainty on $t_{\rm var}$ prevents us from strongly constraining the model parameters. In particular, the Doppler factor δ and the magnetic field B. We thus provide two possible realizations of the model, corresponding to two different values of the Doppler factor ($\delta = 30$ and $\delta = 15$) bracketing the typical range of values found in TeV BL Lac modelling (e.g. Tavecchio et al. 2010).

The physical parameters derived reproducing the SEDs of both source states are reported in Table 3. To model the high state, we consider the quasi-simultaneous X-ray data from February 25 observations ($\delta = 30$) and the assumed simultaneous X-ray spectrum ($\delta = 30$ and $\delta = 15$). The values of the parameters are similar to those inferred for other HBL objects (see e.g. Tavecchio et al. 2010).

The differences between the high and the low states is mainly driven by the value of the Lorentz factor of the electrons dominating the emission at the synchrotron peak, $\gamma_{\rm b}$, which almost doubles from the low to the high state, while the other parameters have almost the same value (except for the electron normalization K that, for the case $\delta = 30$, halves from the low to the high state). As expected (Tavecchio et al. 1998), the magnetic field intensity is inversely proportional to the Doppler factor, being therefore larger in the case $\delta = 15$. B field values of 0.05–0.1 G are commonly derived for HBLs (e.g. Tavecchio et al. 2010).

We also report the power carried by the jet through electrons ($P_{\rm e}$), magnetic field (P_B) and protons ($P_{\rm p}$, derived assuming the presence of one cold proton per emitting electron). We note that while in FSRQ this choice is dictated by energetic requirements, in the case of BL Lac there are no stringent constraints on the composition (e.g. Celotti & Ghisellini 2008). However, this choice has a rather small impact on the derived total power, which is dominated by the leptonic component for both values of δ. The magnetic field and protons appear to contribute less to the jet power, which is mostly carried by the electrons. Its total value $P_{\rm jet} = P_{\rm e} + P_B + P_{\rm p} \sim 10^{44}$ erg s^{-1} is also typical (e.g. Ghisellini et al. 2010). While the jet power carried by the electrons and protons doubles during the source flare, the magnetic field strength is reduced.

The Doppler factors assumed for the SED modelling reported in this paper ($\delta = 15$ and $\delta = 30$) are larger than those typically derived from radio observations by about 1 order of magnitude. This discrepancy is commonly found in the TeV BL Lac population (Blasi et al. 2013). Such so-called Doppler crisis implies that the jet decelerates from the source region to the outer regions where the bulk of the radio emission originates (e.g. Georganopoulos & Kazanas 2003; Ghisellini, Tavecchio & Chiaberge 2005).

The assumed one-zone model, although applied here to the average SED of the low state, is strictly valid only for snapshots, since the travelling and expanding blob is expected to change the emission properties because of adiabatic and radiative losses. As noted, e.g. in Tagliaferri et al. (2008), the emission region may be a standing shock through which the jet plasma continuously passes.

Assuming that the whole emission region $R_{\rm em}$ is causally connected on the observed time-scale, the physical parameters derive a minimal variability time-scale of $t_{\rm var,\,min} = [R_{\rm em} \cdot (1+z)](c \cdot \delta) \sim 0.3\,(0.9)$ d for the high state assuming either the high (low) Doppler factor. The values found are both perfectly compatible with the variability time-scale of 1 d inferred from the VHE light curve.

The SSC model of the quasi-simultaneous data (Fig. 8) implies an increase of the inverse Compton peak by a factor of 3 for the high state SED with respect to the low state. When using the assumed simultaneous X-ray spectrum, such increase is excluded. Considering the assumed simultaneous X-ray data, the SSC model indicates a shift of the synchrotron peak and the inverse Compton peak towards higher frequencies and a synchrotron dominance rather than an equal peak flux of both energy bumps. Such synchrotron dominance is more pronounced when using the high Doppler factor for the modelling.

In comparison to the VHE data from Acciari et al. (2009), the inverse Compton peak is more constrained by the MAGIC data of the high source state. The comparison between the physical parameters obtained from the low state SED observed by MAGIC to MWL observations of 1ES 0806+524 in 2008 March 8 is not straightforward, as Acciari et al. (2009) applied an SSC model whose electron spectrum is approximated by an unbroken power law. The synchrotron and inverse Compton peak positions ($\nu_{\rm sync} \approx 10^{16}$ Hz, $\nu_{\rm IC} \approx 10^{24}$ Hz, corresponding to ∼41 eV and ∼13 GeV) derived for the SED from 2008 (Acciari et al. 2009) and MAGIC observations presented in this paper are located at the same order of frequency.

In contrast to Acciari et al. (2009), our SSC model implies a clear deviation from equipartition (with electrons dominating the total energy density), which is even more pronounced during the high state of the source. The origin of this difference with the VERITAS results is likely due to the different synchrotron peak frequency that, in the case of VERITAS, allowed a larger value of the magnetic field.

5 SUMMARY AND DISCUSSION

In this article, we report on the MAGIC observations of the HBL object 1ES 0806+524 from 2010 December to 2011 June, which were triggered by an optical high state. MAGIC detected a 1 d long flare with a VHE flux three times larger than the flux during the low state. This flaring episode lasted less than 1 d. From this relatively short, high-activity state, whose observation in weak sources like 1ES 0806+524 is rather rare, a short-term variability of 1 d timescale has been inferred. This in turn sets constraints on the size of the emitting region during the high VHE state. Excluding the flare night, the VHE γ-ray flux from the source was in good agreement with the one observed by VERITAS in 2008, when the source was in a lower optical state. We present detailed spectra in the energy range from a few hundred GeV to one TeV, describing both the high and the low VHE state.

We studied the variability patterns of 1ES 0806+524 during the MAGIC VHE γ-ray observations across the available wavebands ranging from radio to VHE γ-rays in order to investigate the possible connection between the emission at different frequencies. The 2D linear regression we carried out did not reveal a connection between the flux levels in any of the possible waveband combinations. Although the VHE observations were optically triggered, no apparent evidence of a short-term correlation was found between these wavebands.

As the multifrequency data cover both the high and the quiescent VHE state activities of 1ES 0806+524, we performed one-zone SSC modelling of the SEDs obtained from the respective data sets assuming two different Doppler factors due to the uncertainty on the variability time-scale. This model could adequately explain the broad-band emission during both source states using physical parameters similar to those from other HBL objects. Non-simultaneity of some of the MWL data hampered detailed studies on the broadband variability of 1ES 0806+524.

ACKNOWLEDGEMENTS

We would like to thank the Instituto de Astrofísica de Canarias for the excellent working conditions at the Observatorio del Roque de los Muchachos in La Palma. The support of the German BMBF and MPG, the Italian INFN, the Swiss National Fund SNF, and the ERDF funds under the Spanish MINECO is gratefully acknowledged. This work was also supported by the CPAN CSD2007-00042 and MultiDark CSD2009-00064 projects of the Spanish Consolider-Ingenio 2010 programme, by grant 268740 of the Academy of Finland, by the Croatian Science Foundation (HrZZ) Project 09/176 and the University of Rijeka Project 13.12.1.3.02, by the DFG Collaborative Research Centers SFB823/C4 and SFB876/C3, and by the Polish MNiSzW grant 745/N-HESS-MAGIC/2010/0.

The *Fermi* LAT Collaboration acknowledges generous ongoing support from a number of agencies and institutes that have supported both the development and the operation of the LAT as well as scientific data analysis. These include the National Aeronautics and Space Administration and the Department of Energy in the United States, the Commissariat à l'Energie Atomique and the Centre National de la Recherche Scientifique/Institut National de Physique Nucléaire et de Physique des Particules in France, the Agenzia Spaziale Italiana and the Istituto Nazionale di Fisica Nucleare in Italy, the Ministry of Education, Culture, Sports, Science and Technology (MEXT), High Energy Accelerator Research Organization (KEK) and Japan Aerospace Exploration Agency (JAXA) in Japan, and the K. A. Wallenberg Foundation, the Swedish Research Council and the Swedish National Space Board in Sweden.

Additional support for science analysis during the operations phase is gratefully acknowledged from the Istituto Nazionale di Astrofisica in Italy and the Centre National d'Études Spatiales in France.

The OVRO 40 m monitoring program is supported in part by NASA grants NNX08AW31G and NNX11A043G, and NSF grants AST-0808050 and AST-1109911.

REFERENCES

Acciari V. et al., 2009, ApJ, 690, L126
Ackermann M. et al., 2012, ApJS, 203, 4
Aharonian F. et al., 2004, A&A, 421, 529
Aharonian F. et al., 2007, ApJ, 664, L71
Aharonian F. et al., 2009, ApJ, 696, L150
Albert J. et al., 2006, ApJ, 648, L105
Albert J. et al., 2007a, Nuclear Instruments and Methods in Physics Research A, 583, 494
Albert J. et al., 2007b, ApJ, 667, L21
Albert J. et al., 2007c, ApJ, 669, 862
Albert J. et al., 2008a, Science, 320, 1752
Albert J. et al., 2008b, Nuclear Instruments and Methods in Physics Research A, 588, 424
Albert J. et al., 2008c, ApJ, 674, 1037
Albert J. et al., 2008d, ApJ, 681, 944
Aleksić J. et al., 2010, A&A, 524, A77
Aleksić J. et al., 2011, ApJ, 729, 115
Aleksić J. et al., 2012a, Astropart. Phys., 35, 435
Aleksić J. et al., 2012b, A&A, 539, A118
Aleksić J. et al., 2012c, A&A, 544, A142
Aleksić J. et al., 2012d, ApJ, 748, 46
Aliu E. et al., 2009, Astropart. Phys., 30, 293
Anderhub H. et al., 2009, ApJ, 704, L129
Arnaud K. A., 1996, in Jacoby G. H., Barnes J., eds, ASP Conf. Ser. Vol. 101, Astronomical Data Analysis Software and Systems V, p. 17
Atwood W. B. et al., 2009, ApJ, 697, 1071
Baars J. W. M., Genzel R., Pauliny-Toth I. I. K., Witzel A., 1977, A&A, 61, 99
Bade N., Beckmann V., Douglas N. G., Barthel P. D., Engels D., Cordis L., Nass P., Voges W., 1998, A&A, 334, 459
Barthelmy S. D. et al., 2005, Space Sci. Rev., 120, 143
Bessell M. S., 1979, PASP, 91, 589
Bessell M. S., Castelli F., Plez B., 1998, A&A, 333, 231
Blandford R. D., Rees M. J., 1974, MNRAS, 169, 395
Blasi M. G. et al., 2013, A&A, 559, A75

Böttcher M., Chiang J., 2002, ApJ, 581, 127
Burrows D. N. et al., 2005, Sci. Space Rev., 120, 165
Celotti A., Ghisellini G., 2008, MNRAS, 385, 283
Costamante L., Ghisellini G., 2002, A&A, 384, 56
de la Calle Pérez I. et al., 2003, ApJ, 599, 909
Domínguez A. et al., 2011, MNRAS, 410, 2556
Finke J. D., Razzaque S., Dermer C. D., 2010, ApJ, 712, 238
Fiorucci M., Tosti G., Rizzi N., 1998, PASP, 110, 105
Fitzpatrick E. L., 1999, PASP, 111, 63
Fomin V. P., Stepanian A. A., Lamb R. C., Lewis D. A., Punch M., Weekes T. C., 1994, Astropart. Phys., 2, 137
Foschini L. et al., 2007, ApJ, 657, L81
Foschini L. et al., 2008, A&A, 484, L35
Franceschini A., Rodighiero G., Vaccari M., 2008, A&A, 487, 837
Gaidos J. A. et al., 1996, Nature, 383, 319
Gehrels N. et al., 2004, ApJ, 611, 1005
Georganopoulos M., Kazanas D., 2003, ApJ, 594, L27
Ghisellini G., Tavecchio F., Chiaberge M., 2005, A&A, 432, 401
Ghisellini G., Tavecchio F., Foschini L., Ghirlanda G., Maraschi L., Celotti A., 2010, MNRAS, 402, 497
Gilmore R. C., Somerville R. S., Primack J. R., Domínguez A., 2012, MNRAS, 422, 3189
Hillas A. M., 1985, in Jones F. C., ed., Proc. 19th ICRC, Vol. 3, La Jolla, p. 445
Horan D. et al., 2004, ApJ, 603, 51
Humphrey P. J., Liu W., Buote D. A., 2009, ApJ, 693, 822
Kalberla P. M. W., Burton W. B., Hartmann D., Arnal E. M., Bajaja E., Morras R., Pöppel W. G. L., 2005, A&A, 440, 775
Li T.-P., Ma Y.-Q., 1983, ApJ, 272, 317
Lombardi S., Berger K., Colin P., Diago Ortega A., Klepser S., 2011, Proc. 32nd ICRC, Vol. 3, Beijing, p. 266
Maraschi L., Tavecchio F., 2003, ApJ, 593, 667
Mariotti M., 2011, ATel, 3192
Mattox J. R. et al., 1996, ApJ, 461, 396
Moralejo A. et al., 2009, Proc. 31st ICRC. Łodz, Poland (arXiv:0907.0943)
Moretti A. et al., 2005, Society of Photo-Optical Instrumentation Engineers (SPIE) Conf. Ser., Vol. 5898, UV, X-Ray, and Gamma-Ray Space Instrumentation for Astronomy XIV. Bellingham, WA, p. 360
Nilsson K., Pasanen M., Takalo L. O., Lindfors E., Berdyugin A., Ciprini S., Pforr J., 2007, A&A, 475, 199
Nolan P. L. et al., 2012, ApJS, 199, 31
Padovani P., Giommi P., 1995, ApJ, 444, 567
Petrov L., Taylor G. B., 2011, AJ, 142, 89
Poole T. S. et al., 2008, MNRAS, 383, 627
Readhead A. C. S., Lawrence C. R., Myers S. T., Sargent W. L. W., Hardebeck H. E., Moffet A. T., 1989, ApJ, 346, 566
Reinthal R., Lindfors E. J., Mazin D., Nilsson K., Takalo L. O., Sillanpää A., Berdyugin A., 2012, J. Phys. Conf. Ser., 355, 012
Richards J. L. et al., 2011, ApJS, 194, 29
Roming P. W. A. et al., 2005, Space Sci. Rev., 120, 95
Schachter J. F. et al., 1993, ApJ, 412, 541
Schlegel D. J., Finkbeiner D. P., Davis M., 1998, ApJ, 500, 525
Stamerra A., Berger K., Lindfors E., Mariotti M., Prandini E., Reinthal R., Schultz C., 2011, Astron. Tel., 3208
Stickel M., Padovani P., Urry C. M., Fried J. W., Kuehr H., 1991, ApJ, 374, 431
Tagliaferri G. et al., 2008, ApJ, 679, 1029
Takalo L. O., Nilsson K., Lindfors E., Sillanp A., Berdyugin A., Pasanen M., 2008, in Aharonian F. A., Hofmann W., Rieger F., eds, AIP Conf. Ser. 1085, 4th Int. Symp. High Energy Gamma-Ray Astronomy. Amer. Inst. Phys., Melville, NY, p. 705
Tavecchio F., Maraschi L., Ghisellini G., 1998, ApJ, 509, 608
Tavecchio F., Ghisellini G., Ghirlanda G., Foschini L., Maraschi L., 2010, MNRAS, 401, 1570
Weymann R. J., Morris S. L., Foltz C. B., Hewett P. C., 1991, ApJ, 373, 23

[1]*IFAE, Campus UAB, E-08193 Bellaterra, Spain*
[2]*Università di Udine, and INFN Trieste, I-33100 Udine, Italy*
[3]*INAF National Institute for Astrophysics, I-00136 Rome, Italy*
[4]*Università di Siena, and INFN Pisa, I-53100 Siena, Italy*
[5]*Croatian MAGIC Consortium, Rudjer Boskovic Institute, University of Rijeka and University of Split, HR-10000 Zagreb, Croatia*
[6]*Max-Planck-Institut für Physik, D-80805 München, Germany*
[7]*Universidad Complutense, E-28040 Madrid, Spain*
[8]*Inst. de Astrofísica de Canarias, E-38200 La Laguna, Tenerife, Spain*
[9]*University of Łódź, PL-90236 Lodz, Poland*
[10]*Deutsches Elektronen-Synchrotron (DESY), D-15738 Zeuthen, Germany*
[11]*ETH Zurich, CH-8093 Zurich, Switzerland*
[12]*Universität Würzburg, D-97074 Würzburg, Germany*
[13]*Centro de Investigaciones Energéticas, Medioambientales y Tecnológicas, E-28040 Madrid, Spain*
[14]*Institute of Space Sciences, E-08193 Barcelona, Spain*
[15]*Università di Padova and INFN, I-35131 Padova, Italy*
[16]*Technische Universität Dortmund, D-44221 Dortmund, Germany*
[17]*Unitat de Física de les Radiacions, Departament de Física, and CERES-IEEC, Universitat Autónoma de Barcelona, E-08193 Bellaterra, Spain*
[18]*Universitat de Barcelona, ICC, IEEC-UB, E-08028 Barcelona, Spain*
[19]*Japanese MAGIC Consortium, KEK, Department of Physics and Hakubi Center, Kyoto University, Tokai University, The University of Tokushima, ICRR, The University of Tokyo, Japan*
[20]*Finnish MAGIC Consortium, Tuorla Observatory, University of Turku and Department of Physics, University of Oulu, Finland*
[21]*Institue for Nuclear Research and Nuclear Energy, BG-1784 Sofia, Bulgaria*
[22]*INAF-Trieste, I-34131 Trieste, Italy*
[23]*Università di Pisa, and INFN Pisa, I-56126 Pisa, Italy*
[24]*ISDC-Science Data Center for Astrophysics, CH-1290 Versoix (Geneva), Switzerland*
[25]*ICREA and Institute of Space Sciences, E-08193 Barcelona, Spain*
[26]*Università dell'Insubria and INFN Milano Bicocca, Como, I-22100 Como, Italy*
[27]*Department of Physics and Astronomy and the Bartol Research Institute, University of Delaware, Newark, DE 19716, USA*
[28]*INAF-IRA Bologna, Via Gobetti 101, I-40129, Bologna, Italy*
[29]*Agenzia Spaziale Italiana (ASI) Science Data Center, I-00044 Frascati (Roma), Italy*
[30]*Istituto Nazionale di Astrofisica-Osservatorio Astronomico di Roma, I-00040 Monte Porzio Catone (Roma), Italy*
[31]*Aalto University Metsähovi Radio Observatory, Metsähovintie 114, FI-02540 Kylmälä, Finland*
[32]*Cahill Center for Astronomy and Astrophysics, California Institue of Technology, Pasaden, CA 91125, USA*
[33]*National Radio Astronomy Observatory, P.O. Box 0, Socorro, NM 87801, USA*
[34]*Department of Physics, Purdue University, 525 Northwestern Ave, West Lafayette, IN 47907, USA*

This paper has been typeset from a TEX/LATEX file prepared by the author.